Structure-function relations of the first and fourth extracellular linkers of the type IIa Na+/Pi cotransporter: II. Substrate interaction and voltage dependency of two functionally important sites

Ehnes, C ; Forster, I C ; Bacconi, A ; Kohler, K ; Biber, J ; Murer, H

Abstract: Functionally important sites in the predicted first and fourth extracellular linkers of the type IIa Na+/Pi cotransporter (NaPi-IIa) were identified by cysteine scanning mutagenesis (Ehnes et al., 2004). Cysteine substitution or modification with impermeant and permeant methanethiosulfonate (MTS) reagents at certain sites resulted in changes to the steady-state voltage dependency of the cotransport mode (1 mM Pi, 100 mM Na+ at pH 7.4) of the mutants. At Gly-134 (ECL-1) and Met-533 (ECL-4), complementary behavior of the voltage dependency was documented with respect to the effect of cys-substitution and modification. G134C had a weak voltage dependency that became even stronger than that of the wild type (WT) after MTS incubation. M533C showed a WT-like voltage dependency that became markedly weaker after MTS incubation. To elucidate the underlying mechanism, the steady-state and presteady-state kinetics of these mutants were studied in detail. The apparent affinity constants for Pi and Na+ did not show large changes after MTS exposure. However, the dependency on external protons was changed in a complementary manner for each mutant. This suggested that cys substitution at Gly-134 or modification of Cys-533 had induced similar conformational changes to alter the proton modulation of transport kinetics. The changes in steady-state voltage dependency correlated with changes in the kinetics of presteady-state charge movements determined in the absence of Pi, which suggested that voltage-dependent transitions in the transport cycle were altered. The steady-state and presteady-state behavior was simulated using an eight-state kinetic model in which the transition rate constants of the empty carrier and translocation of the fully loaded carrier were found to be critical determinants of the transport kinetics. The simulations predict that cys substitution at Gly-134 or cys modification of Cys-533 alters the preferred orientation of the empty carrier from an inward to outward-facing conformation for hyperpolarizing voltages.

DOI: https://doi.org/10.1085/jgp.200409061

Structure–Function Relations of the First and Fourth Extracellular Linkers of the Type IIa Na^+/P_i Cotransporter: II. Substrate Interaction and Voltage Dependency of Two Functionally Important Sites

Colin Ehnes, Ian C. Forster, Andrea Bacconi, Katja Kohler, Jürg Biber, and Heini Murer

Institute of Physiology, University of Zurich, CH-8057 Zurich, Switzerland

ABSTRACT Functionally important sites in the predicted first and fourth extracellular linkers of the type IIa Na^+/P_i cotransporter (NaPi-IIa) were identified by cysteine scanning mutagenesis (Ehnes et al., 2004). Cysteine substitution or modification with impermeant and permeant methanethiosulfonate (MTS) reagents at certain sites resulted in changes to the steady-state voltage dependency of the cotransport mode (1 mM P_i, 100 mM Na^+ at pH 7.4) of the mutants. At Gly-134 (ECL-1) and Met-533 (ECL-4), complementary behavior of the voltage dependency was documented with respect to the effect of cys-substitution and modification. G134C had a weak voltage dependency that became even stronger than that of the wild type (WT) after MTS incubation. M533C showed a WT-like voltage dependency that became markedly weaker after MTS incubation. To elucidate the underlying mechanism, the steady-state and presteady-state kinetics of these mutants were studied in detail. The apparent affinity constants for P_i and Na^+ did not show large changes after MTS exposure. However, the dependency on external protons was changed in a complementary manner for each mutant. This suggested that cys substitution at Gly-134 or modification of Cys-533 had induced similar conformational changes to alter the proton modulation of transport kinetics. The changes in steady-state voltage dependency correlated with changes in the kinetics of presteady-state charge movements determined in the absence of P_i, which suggested that voltage-dependent transitions in the transport cycle were altered. The steady-state and presteady-state behavior was simulated using an eight-state kinetic model in which the transition rate constants of the empty carrier and translocation of the fully loaded carrier were found to be critical determinants of the transport kinetics. The simulations predict that cys substitution at Gly-134 or cys modification of Cys-533 alters the preferred orientation of the empty carrier from an inward to outward-facing conformation for hyperpolarizing voltages.

KEY WORDS: phosphate transport proteins • mutagenesis site directed • cysteine • electrophysiology • transport model

INTRODUCTION

Structure–function studies on membrane transport proteins are used to identify functionally important sites and confirm or establish secondary topological features. The application of the substituted cysteine accessibility method (SCAM) to the renal type IIa Na^+/P_i cotransporter (NaPi-IIa) has enabled us to identify functionally important sites that may constitute part of the transport pathway through the protein (Lambert et al., 2001; Kohler et al., 2002a,b). This involves the first intracellular loop (ICL-1) in the NH_2-terminal half of the protein and the third extracellular loop located in the COOH-terminal half of the protein. The modification of cysteines substituted at these sites in almost all cases led to complete block of the cotransport mode, and in some cases increased the leak mode activity (Kohler et al., 2002b). To continue our study of the functional contribution of predicted transmembrane domain linker regions of NaPi-IIa, we have applied SCAM to the two putative extracellular loops ECL-1 and ECL-4 (Ehnes et al., 2004). Cys substitution at each of nine sites in ECL-1 and six sites in ECL-4 was well tolerated, and $^{32}P_i$ uptake and electrogenic behavior were documented for these mutants (Ehnes et al., 2004). In contrast to our previous studies (Lambert et al., 1999, 2001; Kohler et al., 2002a,b), at the completion of the methanethiosulfonate (MTS) modification reaction, these mutants still exhibited a finite cotransport activity that we attributed to altered steady-state voltage-dependent kinetics (Ehnes et al., 2004). Two mutants were selected for more detailed investigation in this study because their voltage dependency changed in a reciprocal manner depending on whether the novel cysteine was modified or not.

C. Ehnes and I.C. Forster contributed equally to this work.

Address correspondence to Ian C. Forster, Physiologisches Institut, University of Zurich, Winterthurerstrasse 190, CH-8057 Zurich, Switzerland. Fax: 41-1-635 5715; email: IForster@access.unizh.ch

K. Kohler's present address is Laboratory of Morphogenesis and Cell Signaling, UMR144, Institut Curie, Paris, France.

Abbreviations used in this paper: MTS, methanethiosulfonate; MTSEA, 2-aminoethyl MTS hydrobromide; NaPi-IIa, type IIa Na^+/P_i cotransporter; WT, wild type.

J. Gen. Physiol. © The Rockefeller University Press • 0022-1295/2004/11/489/15 $8.00
Volume 124 November 2004 489–503
http://www.jgp.org/cgi/doi/10.1085/jgp.200409061

Unlike for some ion channels, the mechanism by which membrane voltage is transduced into conformational changes for cation-coupled cotransporters is not well understood. The two mutants investigated here offer an opportunity to study this mechanism in a Na^+-coupled cotransport system because they exhibit easily distinguishable characteristics that can be altered in situ by chemical mutagenesis. We interpreted both steady-state and presteady-state analyses to show that the cys substitution and cys modification induce major conformational changes associated with preferred state occupancy of the empty carrier, in agreement with the concept of an alternating access model for cation-coupled electrogenic cotransporters. We further suggest that for NaPi-IIa, these conformational changes lead to an altered access by protons that can interact with voltage-sensitive elements of the NaPi-IIa protein and that the two extracellular linker regions studied here may be involved in major structural rearrangements of the protein during transport.

MATERIALS AND METHODS

The experimental methods and materials used in this study were essentially the same as described in the previous article (Ehnes et al., 2004) with the following additions.

Reagents and Solutions

The solution compositions (in mM) were as follows. (a) Control superfusate (ND100): NaCl (100), KCl (2), $CaCl_2$ (1.8), $MgCl_2$ (1), HEPES-TRIS (10) (for pH 8.0–6.2) or HEPES-MES (10) (for pH 5.6–5.0). For presteady-state protocols, $CaCl_2$ was replaced with equimolar $BaCl_2$ to reduce contamination from endogenous Ca^{2+}-activated Cl^- channels. (b) Control superfusate (ND0): as for ND100 with choline chloride used to replace Na^+. Solutions with intermediate Na^+ concentrations for determining the Na^+ activation kinetics were prepared by mixing ND0 and ND100 in the appropriate proportions or adding the molar equivalent of NaCl for concentrations >100 mM.

Functional Assays and Data Analysis

Steady-state Assays. The P_i activation kinetics were determined at 100 mM Na^+, with six P_i concentrations (total P_i, pH 7.4) in the range 0.01–3 mM P_i; the Na^+ activation kinetics were determined at 1 mM P_i (total P_i, pH 7.4) with six Na^+ concentrations in the range 10–125 mM. The proton dependency was determined using ND100 with pH ranging from 5.0 to 8.0 in 0.6 pH unit increments and total P_i = 1 mM. Voltage dependency of the kinetic parameters was determined using the voltage staircase protocol as previously described (Ehnes et al., 2004), and endogenous oocyte currents were eliminated by subtracting the holding current recorded when the oocyte was superfused in a P_i-free control solution with the same ionic composition as the test solution.

The P_i activation data were fit with a form of the Michaelis-Menten equation:

$$I_{P_i} = I_{P_i}^{max}([P_i]/([P_i] + K_m^{P_i})) + K, \quad (1)$$

where $[P_i]$ is the P_i concentration, $K_m^{P_i}$ is the apparent affinity for P_i, and $I_{P_i}^{max}$ is the maximum cotransport rate. K is a variable offset to take account of the reversal of I_{P_i} that arises from the above subtraction procedure when the net electrogenic activity, contributed by the cotransport and leak modes, is less than the maximum leak activity. The Na^+ activation data were fit with the modified Hill equation:

$$I_{P_i} = I_{P_i}^{max}([Na]^{n_H}/([Na]^{n_H} + (K_m^{Na})^{n_H})) + K, \quad (2)$$

where [Na] is the concentration of Na^+, n_H is the Hill coefficient, K_m^{Na} is the apparent affinity for Na^+, and K is a variable offset, as above. For characterizing proton interactions, Eq. 2 was used with proton concentration substituted for [Na] and $n_H < 0$, to predict the apparent inhibition constant K_i^H for protons.

Presteady-state Relaxations. These were acquired using voltage steps from $V_h = -60$ mV to test potentials in the range −180 mV to +60 mV. Signals were averaged fourfold, sampled at 50 μs/point, and low-pass filtered at 400 Hz. To improve the signal-to-noise ratio, capacitive current subtraction was used to effect partial suppression of the capacitive transient and thereby allow recordings to be made at high gain without distorting the acquired signal due to amplifier clipping. Relaxations were quantified by fitting a decaying double exponential function using a fitting algorithm based on the Chebychev transform supplied with pClamp v. 8 (Axon instruments, Inc.). To resolve the charge movement associated with the exogenous protein, the subtraction method of Hazama et al. (1997) was employed; the fast component, assumed to represent the capacitive oocyte charging, was extrapolated to the step onset and subtracted from the total transient current. For some batches of oocytes it was necessary to apply a linear baseline correction to eliminate contamination from endogenous Cl^- currents activated at depolarizing or hyperpolarizing potentials.

To quantify charge movements, we numerically integrated the component of intramembranous charge movement (Q) attributed to the exogenous protein, commencing ~2.5 ms after the step onset, at which time the membrane was assumed 100% charged. Q–V data were fitted with the Boltzmann relation:

$$Q = Q_{hyp} + Q_{max}/(1 + \exp(-ze(V - V_{0.5})/kT)), \quad (3)$$

where Q_{max} is the maximum charge translocated, Q_{hyp} is the steady-state charge at the hyperpolarizing limit and depends on V_h, $V_{0.5}$ is the voltage at which the charge is distributed equally between each state, z is the apparent valency per cotransporter, e is the elementary charge, k is Boltzmann's constant, and T is the absolute temperature. This model lumps all mobile charges associated with a particular transition into one effective charged particle (valency z) that moves across the whole transmembrane field in one kinetic step (and assuming sharp energy barriers). The voltage dependence of the relaxation time constant ($\tau - V$) obtained from the exponential fitting was further quantified by fitting an equation that incorporates the apparent inward and outward rates for this particle, given by:

$$\tau = 1/(\alpha\exp(-zeV/2kT) + \beta\exp(zeV/2kT)), \quad (4)$$

where α and β are the inward and outward rates, respectively, at $V = 0$ and we assume the barrier is symmetrical within the transmembrane field. Eqs. 3 and 4 were fit to the data by nonlinear regression analysis with Q_{hyp}, Q_{max}, z, $V_{0.5}$, α, and β as free parameters, at T = 293 K. All curve fitting using Eqs. 1–4 was performed using the nonlinear regression analysis available with GraphPad Prism version 3.02/4.02 for Windows (GraphPad Software).

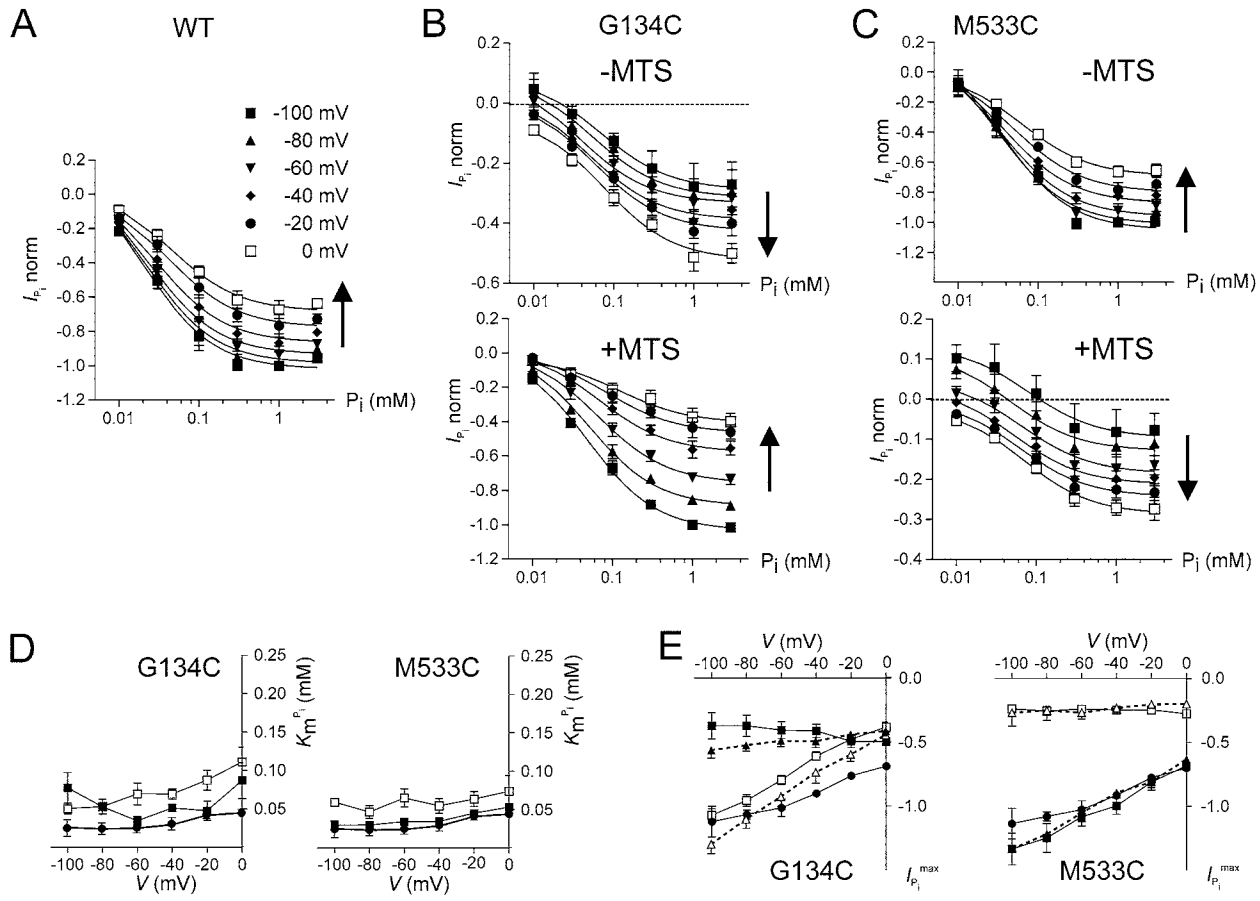

FIGURE 1. Voltage dependency of P_i activation in 100 mM Na^+. (A) P_i activation characteristics for WT-expressing oocytes determined at six membrane potentials from −100 mV to 0 mV as indicated by different symbols. Each data point is the difference between current recorded in ND100 + P_i and ND100 shown as mean ± SEM (n = 3). Currents were normalized to the magnitude of I_{P_i} at 1 mM P_i, V = −100 mV for each cell. Currents for these cells ranged from −76 to −88 nA at 1 mM, V = −100 mV. Arrow indicates direction of depolarization. Continuous lines are fits to the data points using Eq. 1. (B) P_i activation characteristics for G134C-expressing oocytes (n = 4) determined at six membrane potentials as in A, before (top) and after (bottom) incubation in 1 mM MTSEA for 3–5 min. Note the different ordinate scales for the −MTS and +MTS cases. Currents were normalized to the magnitude of I_{P_i} for G134C + MTS at 1 mM P_i, V = −100 mV. Currents for these cells ranged from −22 to −69 nA at 1 mM, V = −100 mV. (C) P_i activation characteristics for M533C-expressing oocytes (n = 4) determined at six membrane potentials as in A before (top) and after (bottom) incubation in 1 mM MTSEA for 3–5 min. Note the different ordinate scales for the −MTS and +MTS cases. Currents were normalized to the magnitude of I_{P_i} for M533C − MTS at 1 mM P_i, V = −100 mV. Currents for these cells ranged from −61 to −123 nA at 1 mM, V = −100 mV. (D) Voltage dependency of apparent P_i affinity ($K_m^{P_i}$) for G134C (left) and M533C (right). Data points indicate mean ± SEM of $K_m^{P_i}$ reported from fits to P_i activation data for the individual oocytes pooled in A–C. WT, filled circles; mutant − MTS, filled squares; mutant + MTS, empty squares. (E) Voltage dependency of predicted maximum P_i-dependent current ($I_{max}^{P_i}$) for G134C (left) and M533C (right) with WT data superimposed. $I_{max}^{P_i}$ is shown as mean ± SEM predicted from fits to data for the individual oocytes pooled in A–C, with WT data superimposed. WT, filled circles; mutant − MTS, filled squares; mutant + MTS, empty squares. Maximum cotransport activity determined using the leak correction procedure (see text) is also shown. Mutant − MTS, filled triangles; mutant + MTS, empty triangles, with points joined by dashed lines.

RESULTS

Voltage Dependency of Apparent Substrate Affinities

In the accompanying cysteine scanning study on mutants in ECL-1 and ECL-4 (Ehnes et al., 2004), we used a simple two-point screening assay to assess if the mutants deviated significantly from the wild type (WT) with respect to substrate activation. This assay was performed at only one membrane potential (−50 mV), and our findings suggested that the cys engineering did not lead to large changes in the apparent substrate affinities. However, it is known that such phenomenological kinetic parameters of NaPi-IIa are functions of membrane potential (Forster et al., 1998). Therefore, to investigate if this could contribute to the novel voltage-dependent behavior of G134C and M533C, we determined the voltage dependency of substrate activation for each mutant before and after 2-aminoethyl MTS hydrobromide (MTSEA) incubation under conditions previously shown to result in

complete modification of the novel cysteines (Ehnes et al., 2004).

Fig. 1 shows the P_i activation data in 100 mM Na^+ for oocytes from the same donor frog that expressed WT (A), G134C (B), and M533C (C). Each panel depicts the normalized P_i-dependent current (I_{P_i}) at different membrane potentials in the range $-100 \leq V \leq 0$ mV. For G134C (Fig. 1 B) and M533C (Fig. 1 C), the same assay was made before (top) and after (bottom) incubation in 1 mM of the MTS reagent MTSEA for 3–5 min. Currents were normalized to the magnitude of I_{P_i} at −100 mV, 1 mM P_i for WT and G134C + MTS and M533C − MTS before pooling. In each case, I_{P_i} displayed saturation for $P_i \geq 1$ mM. Under this condition, the inverse relationship between I_{P_i} and membrane potential for G134C − MTS and M533C + MTS contrasted with the "WT-like" response for G134C + MTS and M533C − MTS, in which increasing hyperpolarization led to increased electrogenic activity. We also observed that for G134C − MTS and M533C + MTS at low P_i, I_{P_i} reversed direction. This is a consequence of subtracting the maximum leak (in ND100) from the current recorded in ND100 + P_i (Forster et al., 1998; Ehnes et al., 2004) (see DISCUSSION). As shown in each panel, the pooled data could be well described by fitting a Michaelis-Menten function with variable offset parameter to account for the sign reversal (Eq. 1). The larger error bars associated with G134C − MTS and M533C + MTS at −100 mV, in particular, most likely arise from the uncertainties in resolving these currents as they were typically <20 nA in magnitude and would be more prone to contamination from endogenous conductances.

To compare the effect of MTS treatment and take account of any systematic errors between individual oocytes, we refit the data of each cell individually (WT, $n = 3$; G134C and M533C, $n = 4$) and pooled the reported estimates of the apparent affinity for P_i interaction with the transporter ($K_m^{P_i}$). These are shown plotted as a function of voltage for G134C (Fig. 1 D, left) and M533C (Fig. 1 D, right) with WT values superimposed for comparison**.** Both mutants showed a relatively weak voltage dependency for $K_m^{P_i}$, as we have previously reported for the WT (Forster et al., 1998). Over the voltage range -100 mV $\leq V \leq 0$ mV, $K_m^{P_i}$ was close to the WT for M533C − MTS. Although the reported mean $K_m^{P_i}$ for M533C + MTS was systematically larger (∼30%) compared with M533C − MTS, a paired t test indicated no significant difference in $K_m^{P_i}$ between M533C − MTS and M533C + MTS ($P < 0.05$). For G134C − MTS, there was more scatter in the $K_m^{P_i}$ estimates because of the smaller currents with no statistical difference from the WT until V approached 0 mV. On the other hand, the mean $K_m^{P_i}$ for G134C + MTS was generally larger than either WT or G134C − MTS, and a paired t test revealed a significant difference ($P < 0.05$) between the respective $K_m^{P_i}$ s of G134C − MTS and G134C + MTS for $V \geq -40$ mV.

Fig. 1 E shows the predicted maximum currents ($I_{P_i}^{max}$) obtained from the fits of the normalized data for G134C (left, squares) and M533C (right, squares), compared with typical WT values (circles). These data showed that with saturating P_i (a) the voltage dependency for G134C − MTS and M533C + MTS was reduced compared with the WT, G134C + MTS, or M533C − MTS, as we previously documented (Ehnes et al., 2004); (b) the voltage dependency $I_{P_i}^{max}$ for M533C was close to the WT; (c) G134C + MTS showed an increased voltage dependency compared with the WT; and (d) at $V = 0$, the predicted $I_{P_i}^{max}$ for G134C − MTS and G134 + MTS were very close, whereas that of M533C + MTS was reduced by ∼70%. Also shown in Fig. 1 E (triangles) is the maximum cotransport mode activity determined by applying the leak correction procedure to I_{P_i} at 3 mM P_i, using the leak estimated from the PFA response as previously described (Ehnes et al., 2004). This agreed reasonably well with the $I_{P_i}^{max}$ predicted from the fits with Eq. 1, particularly for M533C.

Fig. 2 shows the Na^+ activation data at 1 mM P_i for oocytes that expressed WT (A), G134C (B), and M533C (C). Each panel depicts the P_i-dependent current (I_{P_i}) at different membrane potentials in the range $-100 \leq V \leq 0$ mV. As for the P_i activation (Fig. 1), the normalized and pooled data for G134C and M533C are shown before (top) and after (bottom) incubation in 1 mM MTSEA for 3–5 min. The data for G134C + MTS, M533C − MTS, and the WT displayed a similar pattern with a strong voltage dependency at the maximum Na^+ (125 mM) used in these assays. For G134C − MTS and M533C + MTS, the relative P_i currents were suppressed compared with G134C + MTS and M533C − MTS, respectively, and in all cases I_{P_i} showed evidence of saturation with increasing Na^+ concentration. Like the P_i activation data, there was an inverse relationship with voltage for the maximum dependent current, and, moreover, a reversal of I_{P_i} was observed for G134C − MTS and M533C + MTS at low Na^+ concentrations. The data were fit with a form of the modified Hill equation with a variable offset (Eq. 2) to estimate the apparent Na^+ affinity for cotransport (K_m^{Na}) (Fig. 2 D). Reliable fits of Eq. 2 to the WT, G134C + MTS, and M533C − MTS data were obtained with n_H as a free parameter. We found that n_H was reasonably constant when averaged over the estimates at each test potential (WT, 2.0 ± 0.1; G134C + MTS, 1.8 ± 0.1; M533C − MTS, 2.2 ± 0.2). These data confirmed a cooperative Na^+ interaction with the engineered transporters and suggested that for G134C + MTS, the cooperativity was possibly reduced compared with the WT. For the G134C − MTS and M53C + MTS data, where the currents were typi-

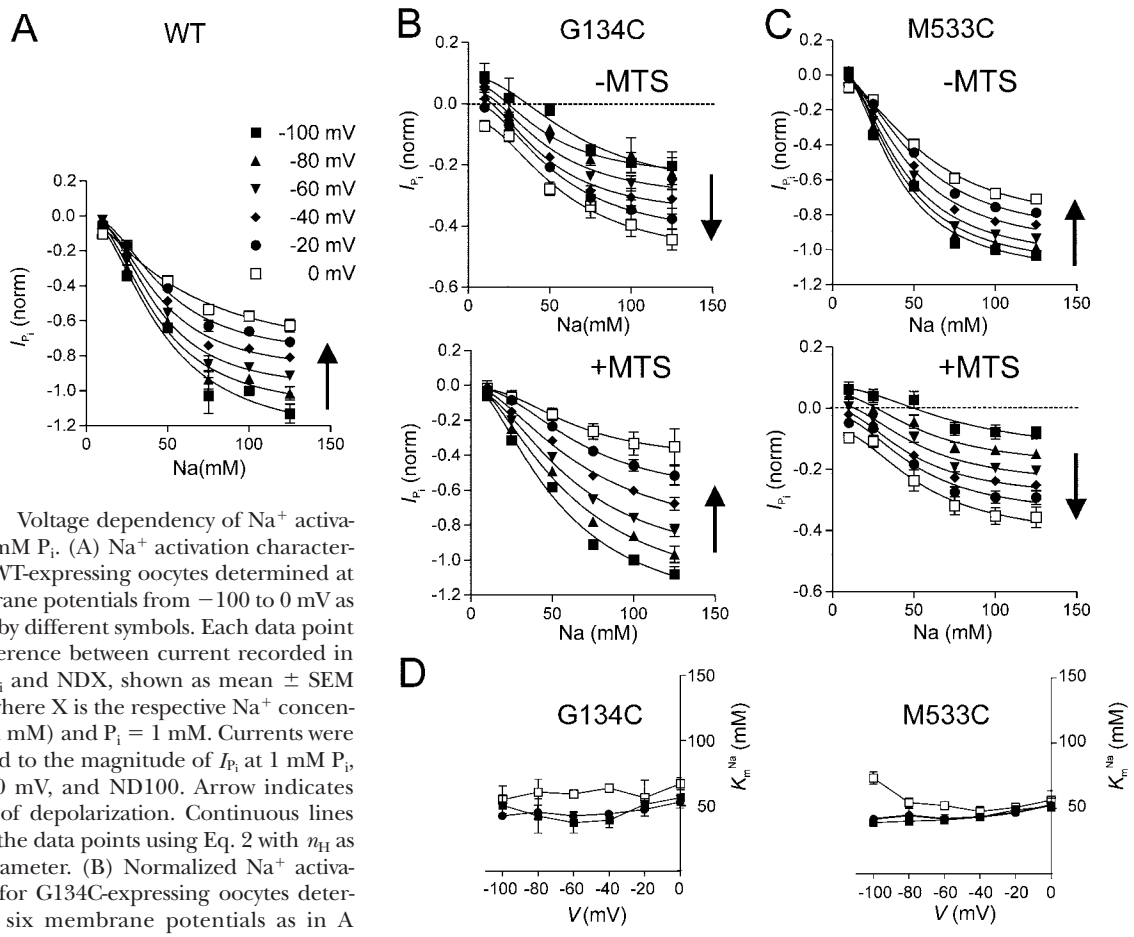

FIGURE 2. Voltage dependency of Na^+ activation in 1 mM P_i. (A) Na^+ activation characteristics for WT-expressing oocytes determined at six membrane potentials from −100 to 0 mV as indicated by different symbols. Each data point is the difference between current recorded in NDX + P_i and NDX, shown as mean ± SEM (n = 4), where X is the respective Na^+ concentration (in mM) and P_i = 1 mM. Currents were normalized to the magnitude of I_{P_i} at 1 mM P_i, V = −100 mV, and ND100. Arrow indicates direction of depolarization. Continuous lines are fits to the data points using Eq. 2 with n_H as a free parameter. (B) Normalized Na^+ activation data for G134C-expressing oocytes determined at six membrane potentials as in A before (top) and after (bottom) incubation in 1 mM MTSEA for 3–5 min. Continuous lines are fits to the data points using Eq. 2 with n_H as a free parameter for G134C + MTS, and n_H = 2 for G134C − MTS. Note the different ordinate scales for the −MTS and +MTS cases. Currents were normalized to the magnitude of I_{P_i} for G134C + MTS, ND100, V = −100 mV. (C) Normalized Na^+ activation data for M533C-expressing oocytes (n = 4) determined at six membrane potentials as in A before (top) and after (bottom) incubation in 1 mM MTSEA for 3–5 min. Continuous lines are fits to the data points using Eq. 2 with n_H as a free parameter for M533C − MTS, and n_H = 2 for M533C + MTS. Note the different ordinate scales for the −MTS and +MTS cases. Currents were normalized to the magnitude of I_{P_i} for M533C − MTS, ND100, V = −100 mV. (D) Voltage dependency of apparent Na^+ affinity (K_m^{Na}) for G134C (left) and M533C (right). Data points indicate mean ± SEM of $K_m^{P_i}$ reported from fits to Na^+ activation data for the individual oocytes pooled in A–C. WT, filled circles; mutant − MTS, filled squares; mutant + MTS, empty squares.

cally <−30 nA, reliable fits of Eq. 2 over the same voltage range were only obtained by constraining n_H = 2.

To compare the effect of MTS treatment on the apparent affinity for Na^+ activation and take account of any systematic errors between individual oocytes, we refit the data of each cell (n = 4) individually and pooled the reported estimates of K_m^{Na}. These are shown as a function of voltage for G134C (Fig. 2 D, left) and M533C (Fig. 2 D, right). For M533C − MTS, K_m^{Na} was indistinguishable from the WT value, although the M533C + MTS data deviated significantly for $V \leq -80$ mV (paired t test, $P < 0.05$). For G134C − MTS, there was no statistically significant deviation from WT. The larger mean K_m^{Na} for G134C + MTS suggested that there was a systematic increase in K_m^{Na}, but this amounted to ∼35% over the entire voltage range and would lie within the normal variation observed among different batches of oocytes.

Proton Interactions with G134C and M533C

The reduced slope and cotransport activity of the *I–V* data for G134C − MTS and M533C + MTS under conditions of maximum turnover rate (Fig. 1 E) were reminiscent of the effect of external acidification on the WT NaPi-IIa P_i-dependent current, whereby protons were shown to reduce its steady-state voltage dependency (Forster et al., 2000). To investigate if an increased sensitivity to external protons could influence the steady-state kinetic changes documented at pH 7.4, we determined the P_i-dependent activity as a function of V and external pH with 1 mM (total) P_i in the pH range 5–8 (Fig. 3).

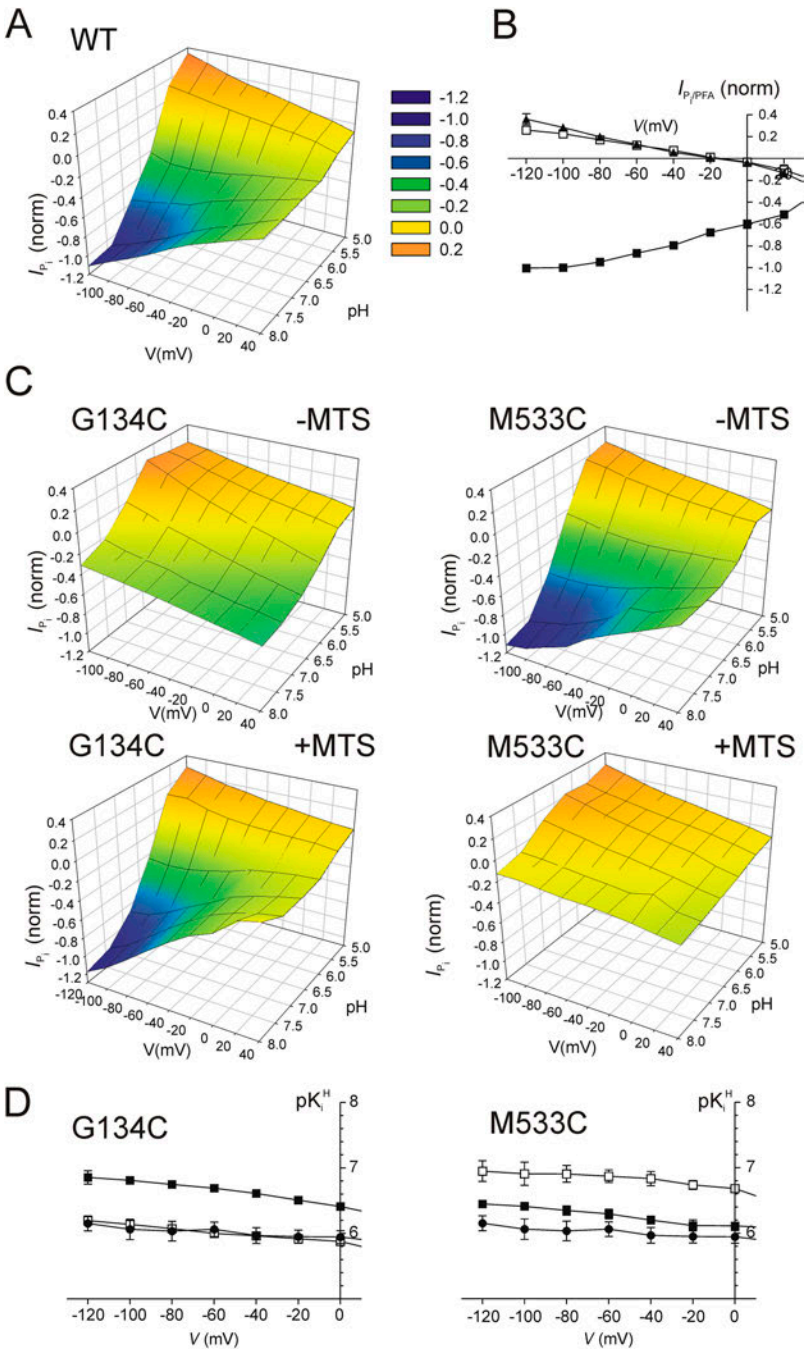

FIGURE 3. Effect of MTS exposure on pH and voltage dependency. (A) Steady-state pH–*V* profile of WT showing I_{P_i} (1 mM total P_i) as a function of external pH and *V*. Currents were normalized to the magnitude of I_{P_i} at −100 mV, pH 7.4, and pooled ($n = 4$). Error bars omitted for clarity. Legend indicates color and corresponding I_{P_i} (norm). (B) Normalized, pooled ($n = 5$) *I–V* data for WT that compares I_{P_i} at pH 5.0 (open squares) with PFA-dependent current at pH 7.4 (filled triangles), normalized to the magnitude of I_{P_i} at −100 mV, pH 7.4 (filled squares). (C) Steady-state pH–*V* profiles of mutant G134C (left) and mutant M533C (right) showing I_{P_i} (1 mM total P_i) as a function of external pH and *V* before (−MTS) and after (+MTS) exposure to 1 mM MTSEA. Currents were normalized to the magnitude of I_{P_i} at −100 mV, pH 7.4, for G134C + MTS and M533C − MTS. Each data point is the mean of four cells from the same donor frog. Error bars omitted for clarity. The assay was repeated after exposure for 5 min to 1 mM MTSEA. Colored contour planes are as in A. (D) Voltage dependency of apparent inhibition constant for protons, K_i^H, (expressed in pH units) for G134C (left) and M533C (right) before (filled) and after (open) exposure to MTSEA. pK_i^H for WT is shown superimposed in both cases (filled circles). Data points were fitted with the modified Hill equation (Eq. 2) with n_H as a free parameter and external proton concentration expressed logarithmically. Error bars indicate SEM of fit estimate for pK_i^H.

For WT NaPi-IIa, over a 3-decade change in external proton concentration, application of P_i evoked an electrogenic response such that with increasing external acidification, the slope of the normalized *I–V* curve changed sign and at pH 5.0, I_{P_i} reversed its dependency on membrane potential (Fig. 3 A). The voltage dependency of I_{P_i} at pH 5.0 appeared similar to the PFA-dependent current measured at pH 7.4, and there was excellent agreement between these currents when measured on the same oocytes and normalized to their respective I_{P_i} at pH 7.4 (1 mM P_i) (Fig. 3 B). These data provided strong evidence that the P_i-dependent current at pH 5.0 was equivalent to the blockage of the leak current that we have previously reported to be pH insensitive (Forster et al., 2000). As expected, we also documented that at pH 5.0, $^{32}P_i$ uptake by WT NaPi-IIa was negligible when compared with the background (unpublished data). Taken together, these results established that at pH 5.0, P_i interacted with the transporter, but the cotransport mode was fully suppressed.

As shown in Fig. 3 C, G134C and M533C displayed complementary pH–*V* profiles under the same experi-

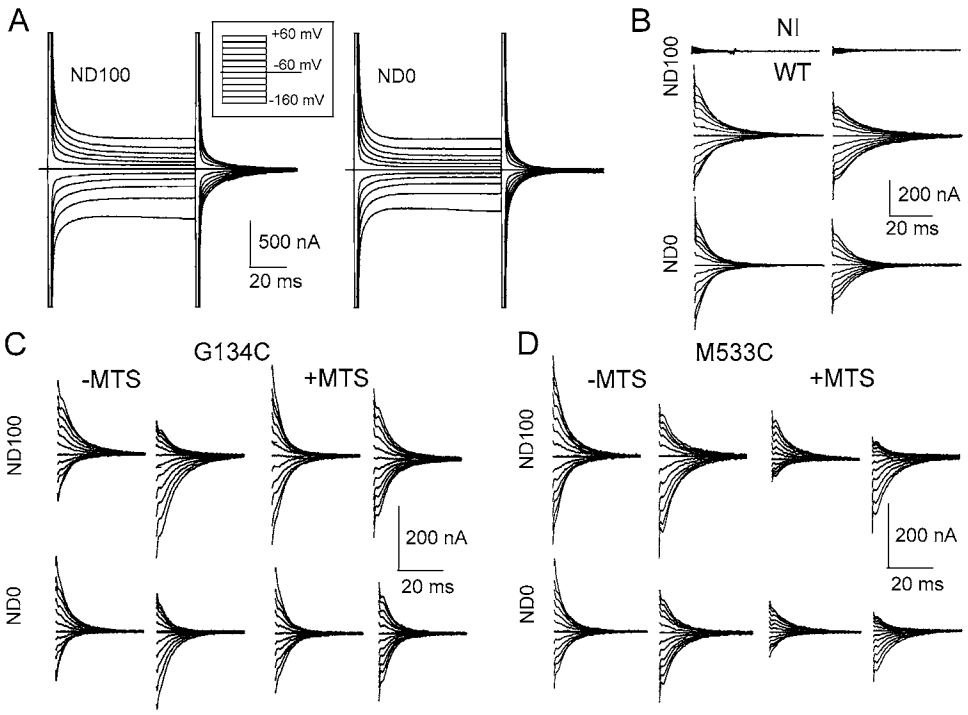

FIGURE 4. Effect of MTS exposure on presteady-state relaxations of mutants. (A) Representative presteady-state relaxations recorded from an oocyte expressing the WT NaPi-IIa protein superfused in 100 mM Na^+ (ND100) and 0 mM Na^+ (ND0) for the voltage step protocol shown in the inset. (B) Main component of presteady-state relaxation for a noninjected oocyte (NI) and the same WT-expressing cell in *A*, resolved by applying a two-exponential fitting procedure (see MATERIALS AND METHODS). The ON (step from −60 mV to test potential) and OFF (step from test potential to −60 mV) relaxations are shown for superfusion in ND100 (top and middle traces) and ND0 (bottom traces). (C) Main ON and OFF relaxations for a representative G134C-expressing oocyte before (−MTS) and after (+MTS) exposure to 1 mM MTSEA (1 mM) for 3 min, superfused in ND100 and ND0. (D) Main ON and OFF relaxations for a representative M533C-expressing oocyte before (−MTS) and after (+MTS) exposure to 1 mM MTSEA (1 mM) for 3 min, superfused in ND100 and ND0.

mental conditions. Over a 3-decade range in external proton concentration, the pH–*V* profiles of G134C + MTS and M533C − MTS were similar to WT, whereas for G134C − MTS and M533C + MTS, the inverse voltage dependency and reduced activity, already documented at pH 7.4, were preserved. Like the WT, a consistent feature of the pH–*V* profiles was a close agreement between I_{P_i} at pH 5.0 and I_{PFA} (unpublished data). To quantify the proton interactions before or after MTS modification, we fit the *I–V* data with the modified Hill equation (Eq. 2) with protons as the variable substrate, to obtain an apparent inhibition constant (K_i^H) for each test voltage (Fig. 3 D), with K_i^H expressed in pH units (pK_i^H). pK_i^H was a weak function of *V* and increased slightly at hyperpolarizing potentials, with the largest change (0.4 pH units) for G134C − MTS and smallest for the WT (∼0.1 pH units). Over the voltage range examined, pK_i^H for G134C + MTS was indistinguishable from the WT, whereas pK_i^H for G134C − MTS increased by ∼0.7 pH units. We documented reciprocal behavior for M533C, although pK_i^H for M533C − MTS itself was ∼0.3 pH units higher than the WT. The predicted n_H from these fits for WT, G134C + MTS, and M533C − MTS decreased from ∼−1 at $V = -100$ mV to ∼−2 at $V = 0$. For G134C − MTS and M533C + MTS, n_H increased in a complementary manner. These findings suggested that cys substitution at Gly-134 and modification of Cys-533 had altered the cooperativity of proton interactions compared with the WT. Moreover, they provided evidence of an increased sensitivity to external protons for G134C − MTS and M533C + MTS. Nevertheless, for G134C − MTS or M533C+MTS, removal of external protons did not restore the level of P_i-dependent electrogenic activity to that of the WT. This can be seen from their pH–*V* profiles and from the predicted extrapolated current, as pH → ∞, obtained from the fits (unpublished data). This indicated that the cys engineering had induced changes in the transporter kinetics that were independent of the proton interactions.

Presteady-state Charge Distributions of G134C and M533C

To gain further insight into underlying molecular mechanisms associated with the altered steady-state *I–V* data of the G134C/M533C pair, we investigated if changes also occurred to the kinetics of the presteady-state charge movements that accompany rapid changes in membrane potential. These experiments were all performed at pH 7.4 in the absence of P_i. Fig. 4 A depicts presteady-state relaxations in ND100 and ND0 for a representative WT-expressing oocyte in response to the voltage step protocol shown (Fig. 4 A, inset). These relaxations were superimposed on the oocyte capacitive charging transients and were not observed for noninjected oocytes under the same conditions (unpublished data). Fig. 4 B shows the presteady-state relax-

TABLE I

Boltzmann Fit Parameters

	−MTSEA		+MTSEA	
	ND0	ND100	ND0	ND100
G134C				
α (s^{-1})[a]	31 ± 3	37 ± 3	22 ± 2	19 ± 1
β (s^{-1})[a]	60 ± 4	52 ± 3	123 ± 5	109 ± 5
z[a]	0.5 ± 0.04	0.4 ± 0.04	0.5 ± 0.03	0.5 ± 0.03
$V_{0.5}$ (mV)[b]	−2 ± 3	+6 ± 3	−69 ± 6	−86 ± 5
z[b]	0.5 ± 0.02	0.5 ± 0.01	0.4 ± 0.04	0.4 ± 0.02
M533C				
α (s^{-1})[a]	28 ± 1	24 ± 1	37 ± 3	36 ± 3
β (s^{-1})[a]	74 ± 3	56 ± 2	43 ± 3	42 ± 3
z[a]	0.4 ± 0.02	0.4 ± 0.02	0.5 ± 0.04	0.4 ± 0.05
$V_{0.5}$ (mV)[b]	−42 ± 11	−28 ± 8	+16 ± 13	+22 ± 4
z[b]	0.5 ± 0.03	0.5 ± 0.02	0.5 ± 0.06	0.6 ± 0.02

[a]Mean ± SEM of fit pooled τ–*V* data (n = 4) using Eq. 4.

[b]Mean ± SEM of pooled data from fits to individual *Q*–*V* data (n = 4) using Eq. 3.

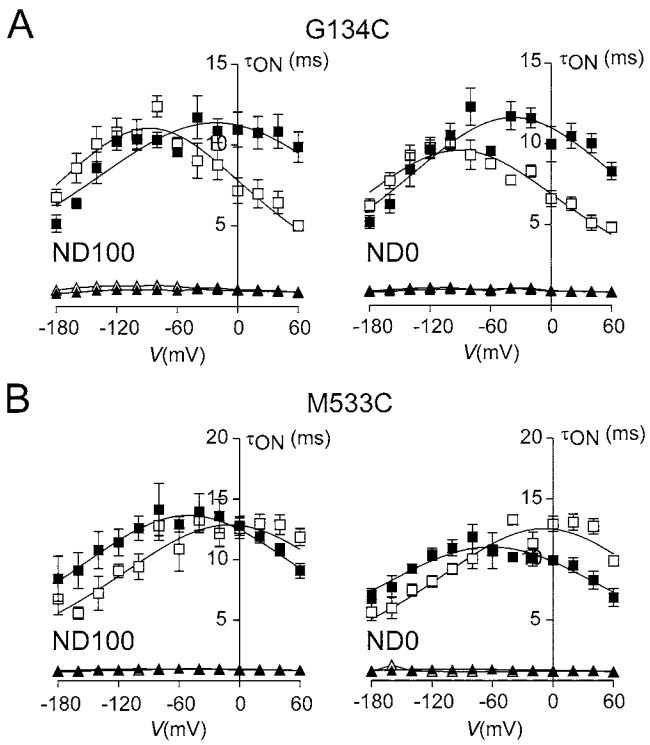

FIGURE 5. Analysis of presteady-state relaxations; ON time constants (τ_{ON}) for mutant G134C (A) and M533C (B). Voltage dependencies of time constants (τ_{ON}) were obtained by fitting presteady-state relaxations in response to voltage steps from −60 mV to the indicated voltage with a double exponential (see MATERIALS AND METHODS). Each point represents mean ± SEM of four cells. Fast τ_{ON} (triangles), slow τ_{ON} (squares); before MTSEA (filled symbols); after MTSEA (empty symbols) incubation (1 mM, 3 min). Continuous lines were obtained by fitting Eq. 4 to the data (Table I). Data for two superfusion conditions: ND100 (left) and ND0 (right). Data points at the holding potential (−60 mV) were determined from fits to the OFF relaxations.

ations for the ON (step from −60 mV to test potential) and OFF (step from test potential to −60 mV) on an expanded scale, after removing the capacitive charging transient and holding current (see MATERIALS AND METHODS) for the same cell as in A. For comparison, the same data manipulation procedure applied to a noninjected oocyte (NI) from the same donor frog showed no detectable charge movement within the same time window (top traces, ND100 superfusion only). The relaxations appear almost symmetrically distributed around the baseline trace at V_h = −60 mV because for the WT rat NaPi-IIa, the midpoint potential ($V_{0.5}$) of the charge distribution typically lies in the range −70 to −50 mV (e.g., Forster et al., 1998, 2000), i.e., $V_h \cong V_{0.5}$.

Representative voltage step–induced currents recorded before (−MTS) and after (+MTS) exposure to MTSEA (1 mM, 3 min) for G134C and M533C are shown in Fig. 4 (C and D), respectively. For ND100 superfusion, G134C-expressing oocytes showed an altered charge distribution around V_h = −60 mV, from an asymmetrical form before MTS exposure to a more WT-like symmetrical distribution (Fig. 4 B) after treatment. This behavior was also documented in 0 mM external Na^+ (ND0). In contrast, M533C showed the opposite behavior, whereby a WT-like symmetrical charge distribution became more asymmetrical after MTS treatment, also for ND0 superfusion. We also observed qualitatively similar results for MTSET- and MTSES-treated oocytes (unpublished data). These findings indicated that the intrinsic charge of the MTS reagent was not critical for inducing changes in the kinetics.

The faster component for both ON and OFF transitions had a time constant (τ) ~1 ms and showed little voltage dependency, and we therefore assumed that it arose primarily from the capacitive charging of the oocyte membrane. The slower ON component showed a strong voltage dependency that changed after MTS treatment, as evidenced by the shift in the peak τ from ~0 to −60 mV. We quantified these changes by fitting the τ–*V* data with an equation for relaxations derived from a two-state Boltzmann model (Eq. 4) (Table I). The two mutants showed complementary behavior, as suggested by the presteady-state records in Fig. 4 (C and D). For G134C + MTS (Fig. 5 A) with superfusion in either ND100 or ND0, there was a shift of the peak in the hyperpolarizing direction, whereas for M533C + MTS (Fig. 5 B), shifts in the depolarizing direction were found for both ND100 and ND0. In each case, exponential curve fitting of the OFF transition resolved a slow component that was only weakly voltage dependent (unpublished data). We would expect this for a system in which the reaction rate is dependent on the target potential. The parameters derived from the fits to Eq. 4 (Table I) indicated that for a given superfusion

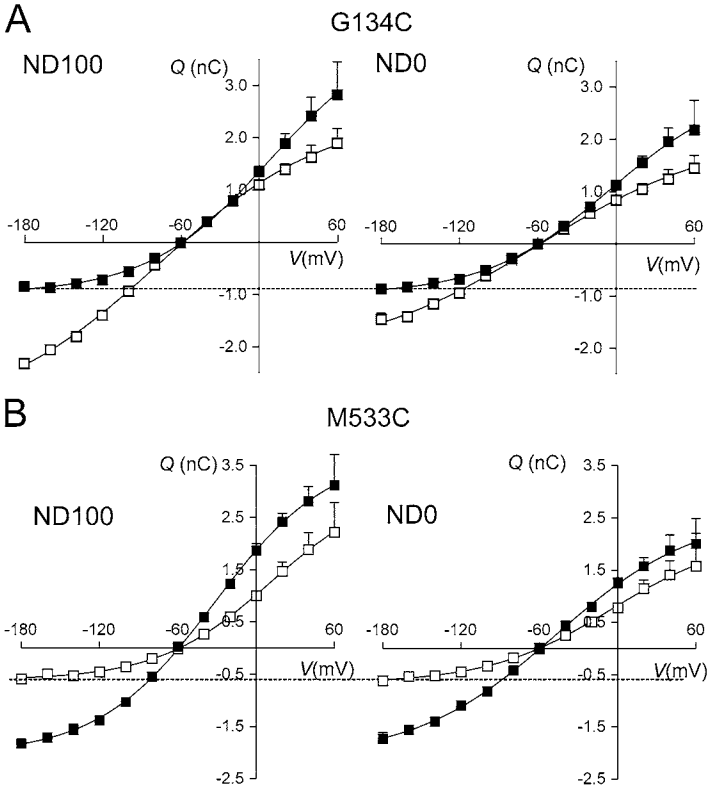

FIGURE 6. Analysis of presteady-state relaxations: charge–voltage (Q–V) data for a representative oocyte expressing G134C (A) and M533C (B). Each point is given by $(Q_{ON}-Q_{OFF})/2$, where Q_{ON} and Q_{OFF} are the charges moved for the ON and OFF voltage steps from and to −60 mV, respectively. Errors smaller than symbol size are not shown. Left, superfusion in ND100; right, superfusion in ND0 for the same oocyte. Filled symbols, before MTSEA exposure; empty symbols, after MTSEA exposure. Dashed lines have been drawn to indicate the apparent equality of charge movement at hyperpolarizing potentials for ND100 and ND0 superfusion for G134C − MTS and M533C + MTS. Continuous lines were obtained by fitting Eq. 3 to the data. For G134C, the fit parameters were as follows: in ND100 (±MTS), Q_{max} = 5.1/5.9 nC, Q_{hyp} = −0.9/−3.4 nC; $V_{0.5}$ = −7/−77 mV; z = 0.5/0.4; and in ND0 (±MTS), Q_{max} = 4.0/4.3 nC, Q_{hyp} = −1.0/−2.1 nC; $V_{0.5}$ = −5/−59 mV; z = 0.5/0.4. For M533C, the fit parameters were as follows: in ND100 (±MTS), Q_{max} = 5.8/3.7 nC, Q_{hyp} = −2.0/−0.7 nC; $V_{0.5}$ = −32/+11 mV; z = 0.6/0.6; and in ND0 (±MTS), Q_{max} = 4.8/2.9 nC, Q_{hyp} = −2.1/−0.6 nC; $V_{0.5}$ = −48/−5 mV; z = 0.5/0.5.

condition, the apparent rate constants at 0 mV showed the greatest sensitivity with respect to MTS treatment, whereas the estimated apparent valency remained reasonably constant.

Fig. 6 A shows the charge–voltage (Q–V) relationship for a representative G134C-expressing oocyte for superfusion in ND100 and ND0 before and after MTS exposure. Each point represents the mean of the absolute charge moved after the ON and OFF transitions.[1] Before MTS exposure, saturation was clearly observed at hyperpolarizing potentials for both ND100 and ND0, and, moreover, the charge moved for steps to potentials $< V_h$ was the same for both ND100 and ND0. After MTSEA exposure, the charge distribution showed a clear difference between superfusion in ND100 and ND0 for hyperpolarizing potentials as well as less saturation in this voltage range. The Q–V data for a representative M533C-expressing oocyte showed the opposite behavior (Fig. 6 B). Before MTS exposure there was a small difference in charge movement between ND100 and ND0, and evidence of saturation was observed at both hyperpolarizing and depolarizing extremes. After MTS exposure, there was much stronger saturation for hyperpolarizing steps with equality of charge movement for the two superfusion conditions, as for G134C − MTS. To quantify these changes, the Q–V data were fit with a Boltzmann function (Eq. 3), and the fitting results pooled (n = 4) for each mutant are summarized in Table I. The fitted data showed reasonable agreement between the predicted apparent valency (z) derived from the Q–V (Eq. 3) or τ–V (Eq. 4) fits. This parameter also remained reasonably constant before and after MTS treatment and suggested that the treatment had not altered the intrinsic voltage sensitivity of the protein, but only its voltage dependency. For G134C − MTS and M533C + MTS, the ratio of the predicted hyperpolarizing charge derived from the Boltzmann fit in ND100 to that in ND0 ($Q_{hyp}^{100}/Q_{hyp}^{0}$) was unity as suggested from the Q–V data. For the G134C +

[1]Charge balance (equality between ON (QON) and OFF (QOFF) charge movements, as demanded by charge conservation) was excellent in the voltage range ($-180 \le V \ge 0$ mV) with a deviation ≤10% (Fig. 6). This confirmed that in this voltage window, all of the charge moved that was associated with the slow relaxation could be recovered. For $V > +20$ mV, the difference increased. An underestimate in QON could result from our inability to detect all charge movement for depolarizing ON transitions because of the limited time window, i.e., uncertainties in the first 2.5 ms after the step onset during the capacitive charging led us to ignore charge movement during this initial interval. Alternatively, very slow charge movements that require a longer time window to resolve might remain undetected or masked by contamination from endogenous Cl^- currents. Although we cannot fully exclude contamination from endogenous membrane proteins in injected oocytes, we were unable to detect charge imbalance in noninjected oocytes (Fig. 4 B). Moreover, in our hands, contributions to charge movement from the endogenous Na^+/K^+-ATPase (e.g., Rakowski, 1993) were considered insignificant as we were unable to detect any change in the presteady-state relaxations after incubating selected cells in 100 mM ouabain, a potent blocker of this pump.

MTS, the ratio >1 confirmed that additional mobile charge was available in the presence of external Na^+. For M533C, $Q_{hyp}^{100}/Q_{hyp}^{0}$ remained close to unity before and after MTS exposure.

DISCUSSION

We have focused on the electrogenic behavior of two mutant NaPi-IIa cotransporters (G134C and M533C) that contain a novel Cys at site Gly-134 in the first predicted extracellular linker (ECL-1) and one at site Met-533 in the fourth predicted extracellular linker (ECL-4), respectively. In an accompanying study (Ehnes et al., 2004), we established that (a) these and other substituted cysteines in ECL-1 and ECL-4 were accessible from the external hydrophilic environment and (b) the voltage-dependent kinetics of G134C and M533C, in particular, were profoundly altered compared with the WT fingerprint. This depended on whether or not the novel Cys was modified by external MTS reagents; G134C + MTS and M533C − MTS showed "WT-like" characteristics, whereas G134C − MTS and M533C + MTS showed weaker voltage dependency that suggested rate-limiting behavior at hyperpolarizing potentials. Moreover, the effect of cys modification on the voltage dependency was independent of the charge of the MTS reagent. The aim of this study was to identify the kinetic transitions that were affected by the cysteine engineering and develop structure–function relationships for these linkers.

We used the eight-state kinetic scheme for NaPi-IIa depicted in Fig. 7 A to relate the functional effects of the cys engineering to specific partial reactions in the overall transport cycle. This model, derived from studies on the WT (Forster et al., 1998, 2000), accounts for voltage-dependent cotransport through two processes: (1) the movement of intrinsic mobile charges in response to changes in the transmembrane electric field, which exposes a Na^+ binding site, and (2) the movement of one Na^+ ion within the transmembrane field to this site (Fig. 7 A, transitions 1–8 and 1–2, respectively). Presteady-state charge movements measured in the absence of external Na^+ result from empty carrier conformational changes, whereas in the presence of external Na^+, additional charge movement is contributed by Na^+ binding/debinding (Forster et al., 1997, 1998). The model includes the minimum possible number of states to account for NaPi-IIa kinetics.

Substrate and Proton Interactions in the Steady State

The steady-state assays revealed a unique characteristic of the P_i-dependent currents, namely the reversal of I_{P_i} documented at hyperpolarizing potentials for G134C − MTS and M533C + MTS in the P_i and Na^+ activation assays at low P_i and Na^+, respectively (Figs. 1 and 2), and for the WT and both mutants at low pH (Fig. 3). This results from the subtraction procedure used to obtain I_{P_i} and the presence of a leak mode that also contributes to the electrogenic response, in addition to the cotransport mode. We have previously proposed that these modes are reciprocally related, so that in 0 mM P_i, maximum leak activity occurs, whereas at saturating P_i, the leak is fully suppressed and only the cotransport mode contributes to electrogenic activity (Kohler et al., 2002b). At intermediate P_i, the P_i-dependent electrogenic activity will comprise components from both modes; however, the relative contributions to the measured P_i-dependent currents remain to be determined. Moreover, Na^+ acting as a common cation complicates the experimental separation of the two transport modes at intermediate P_i. In the case of WT NaPi-IIa, where the leak accounts for ~10% of total electrogenic activity (Forster et al., 1998) at pH 7.4, its effect is usually ignored. Under these conditions, I_{P_i}, obtained from the subtraction procedure, is typically inward for $V < 0$ mV, and the activation kinetics can be well described by fitting data using the Michaelis-Menten equation. However, in general, we would not expect the P_i dependency of the net electrogenic activity to follow a strict Michaelis-Menten characteristic, unless the activation of cotransport and deactivation of leak by P_i are strictly reciprocal. For example, if P_i suppressed the leak with a higher affinity than it activated the cotransport mode, so that at low P_i the magnitude of the combined cotransport and leak activity is less than the maximum leak activity, the subtraction procedure would yield apparent outward currents, as we have documented. This dual interaction of P_i with NaPi-IIa suggests the existence of two binding sites for P_i, but at present, we have no supporting structure–function evidence.

Given the uncertainties concerning the leak dependency on P_i and Na^+, we found that the most straightforward approach to account for the current reversal of the P_i and Na^+ activation kinetics was to fit the data using the standard Michaelis-Menten (Eq. 1) or modified Hill equations (Eq. 2) with a variable offset. The $I_{P_i}^{max}$ predicted from the fits to the P_i activation data agreed reasonably well with the maximum cotransport activity determined using the leak-correction procedure. This suggested that any errors introduced by the P_i-dependent leak component were not significant under our experimental conditions for characterizing the cotransport kinetics.

From the steady-state P_i and Na^+ activation assays, we documented relatively small deviations from the WT behavior for the apparent substrate affinities (K_m^{Na} and K_m^{Pi}) in the voltage range $-100 \leq V \leq 0$ mV, independent of the state of modification of the novel Cys. Deviations reported by the fitting procedure would not be

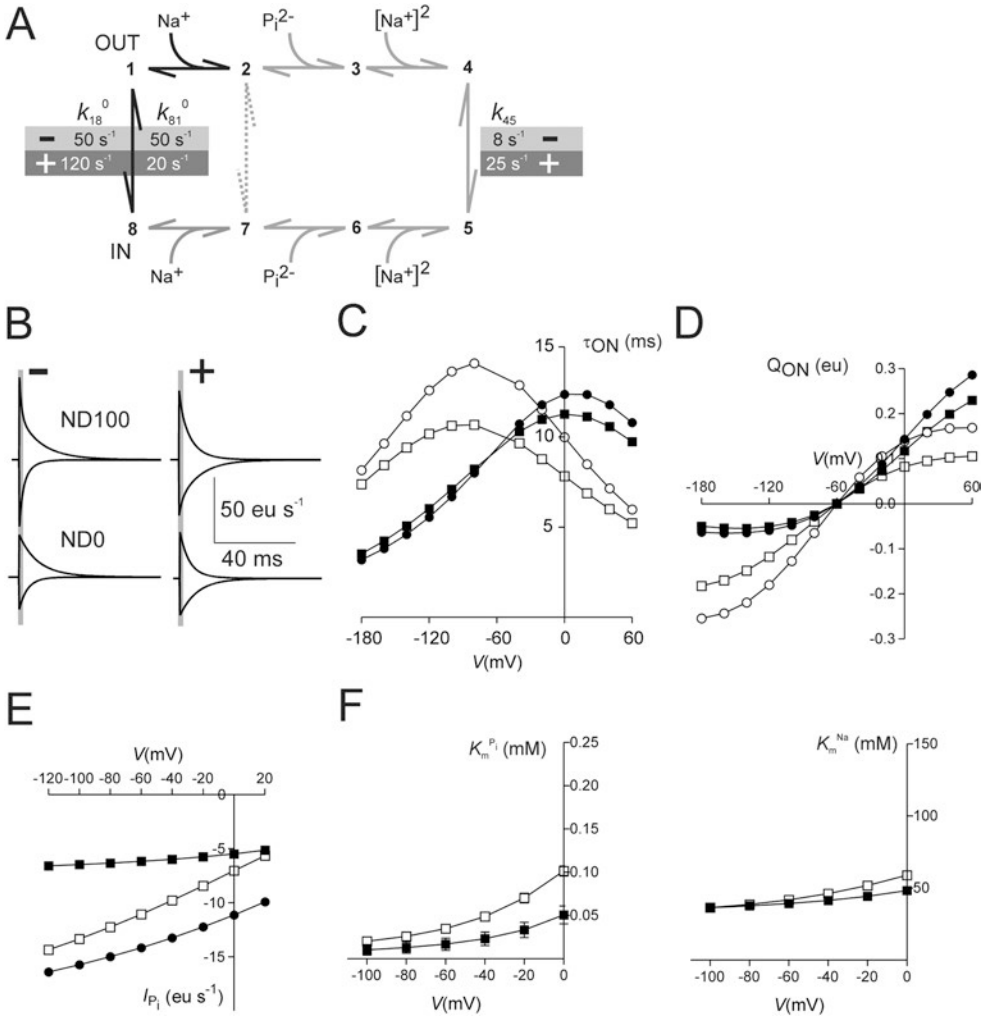

FIGURE 7. Modeling voltage-dependent presteady-state and steady-state kinetics for G134C − MTS and G134C + MTS. (A) Eight-state kinetic scheme for NaPi-IIa. Voltage-dependent transitions are shown bold. All other transitions are electroneutral. Critical transitions for simulating G134C − MTS (−) and G134C + MTS (+) are 1–8, 8–1, and 4–5. The corresponding voltage-independent rates used in the simulations are indicated. Dashed transition indicates a proposed leak pathway. (B) Simulations of presteady-state relaxations before (−) and after (+) MTS modification of Cys-134 using the model scheme of A for steps to potentials in the range −180 to +80 mV from V_h = −60 mV and two superfusion conditions. The vertical gray bars indicate the initial 2.5-ms interval after which presteady-state currents were resolved experimentally. Differential equations describing the transitions were solved for the state occupancies as a function of time. The presteady-state current per cotransporter molecule can be expressed as $-e(\alpha'(k_{12}X_1 - k_{21}X_2) - \delta^*(k_{18}X_1 - k_{81}X_8) + \alpha''(k_{78}X_7 - k_{87}X_8))$ (e.g., Parent et al., 1992), where X_n is the occupancy of state n and k_{ij} is the transition rate from state i to state j. The empty carrier (1–8) carries an equivalent charge of −1 that moves an equivalent electrical distance δ through the membrane. The Na^+ binding transitions (1–2 and 8–7) also involve movement of +1 charge through equivalent electrical distances α' and α'', respectively. To simplify the simulations, $\alpha'' = 0.3$, $\alpha' = 0.3$, and $\delta = 0.4$ and the corresponding energy barriers were symmetrical. The rate constants for voltage-dependent transitions are given by $k_{18} = k_{18}^o \exp(\delta eV/2kT)$, $k_{81} = k_{81}^o \exp(-\delta eV/2kT)$, $k_{12} = \text{Na}\ k_{12}^o \exp(-\alpha' eV/2kT)$, $k_{21} = k_{21}^o \exp(\alpha' eV/2kT)$, where k_{ij}^o is the rate constant for transition ij at $V = 0$, and Na is the concentration of Na^+ (mM). Other fixed rate constants for the simulations were $k_{12}^o = 2000\ s^{-1}M^{-1}$, $k_{21}^o = 600\ s^{-1}$, $k_{23} = 7.5 \times 10^6\ s^{-1}M^{-1}$, $k_{32} = 1000\ s^{-1}$, $k_{34} = 10^6\ s^{-1}M^{-2}$, $k_{43} = 1000\ s^{-1}$, $k_{54} = 25\ s^{-1}$, $k_{78} = 100$, $k_{87} = 10^6\ s^{-1}M^{-1}$, $k_{67} = 1000\ s^{-1}$, $k_{76} = 10^6\ M^{-1}s^{-1}$, $k_{65} = 10^5\ s^{-1}M^{-2}$, $k_{56} = 1000$, $k_{23} = 0.005\ s^{-1}$. To satisfy microscopic reversibility, k_{32} and k_{76} were defined in terms of the other rate constants. (C) Predicted τ–V data was obtained by applying a single exponential fit to the ON presteady-state currents for voltages in the range −180 to +60 mV, commencing 2.5 ms after the step onset. Filled symbols, −MTS; open symbols, +MTS; circles, ND100; squares, ND0. Model parameters are as given in A and B above for the −MTS and +MTS conditions with $P_i = 0$. (D) Predicted Q–V data obtained by numerical integration of the presteady-state currents, commencing 2.5 ms after the step onset. Filled symbols, −MTS; open symbols, +MTS; circles, ND100; squares, ND0. Model parameters are as given in A and B above for the −MTS and +MTS conditions with $P_i = 0$. (E) Predicted steady-state I–V data for the −MTS (filled squares) and +MTS (*open squares*) conditions, using rate constants given in A and assuming $P_i = 1$ mM and external $Na^+ = 100$ mM. The steady-state current is proportional to $k_{14}X_1 - k_{41}X_4$, i.e., the net flux for the only transition that involves transmembrane charge movement. Filled circles represent the simulated I–V data without changing k_{45} (see text). (F) Apparent substrate affinities for P_i activation ($K_m^{P_i}$) (left) and Na^+ activation (K_m^{Na}) (right) as a function of membrane potential. $K_m^{P_i}$ was obtained from a fit using the Michaelis-Menten equation (Eq. 1) to the steady-state activation data simulated with P_i in the range 0–3 mM and $Na^+ = 100$ mM. K_m^{Na} was obtained from a fit using the modified Hill equation (Eq. 2) with Na^+ in the range 0–125 mM and $P_i = 1$ mM. Filled symbols, −MTS; open symbols, +MTS. Error bars indicate ±SEM reported by fitting algorithm.

able to account for the dramatic change in both voltage dependency and maximum transport activity caused by the cys engineering. We therefore excluded transitions 2–3 and 3–4 (Fig. 7 A), previously found to be critical determinants of these parameters (Forster et al., 1998, 2000), from further consideration. On the other hand, we found that the sensitivity of the transporter to protons changed depending on the state of modification

of the substituted Cys (Fig. 3 D). The apparent proton inhibition constants for G134C − MTS and M533C + MTS were smaller than for the WT, which suggested that cys substitution at Gly-134 or cys modification at Met-533 had induced a conformation in which protons could more easily modify the kinetics. For the WT, we have previously identified the empty carrier and final Na^+ binding transitions to be proton sensitive (Forster et al., 2000). The latter interaction, in which protons compete with Na^+ ions (Fig. 7 A, transition 3–4), manifests itself as an approximately twofold increase in K_m^{Na} (e.g., Hartmann et al., 1995) with external acidification. That we did not observe a large change in K_m^{Na} for either mutant suggests that the interaction of protons with the last Na^+ binding transition had not been affected by the cys engineering. Moreover, as reducing the external proton concentration did not in itself restore the WT-like activity for G134C − MTS or M533C + MTS, this suggested that the cys engineering at these sites had affected transitions in the transport cycle that were proton insensitive. Moreover, the depolarizing shift in the presteady-state Q–V and τ–V data, documented for G134C − MTS and M533C + MTS in ND0, was remarkably similar to the effect of external acidification on the WT presteady-state relaxations also in ND0 (Forster et al., 2000), which were shown to result in a weaker steady-state voltage dependency. We therefore focused our attention on the empty carrier to explain the changes in voltage-dependent kinetics.

Simulations Confirm Influence of Empty Carrier Kinetics on Voltage Dependency

To demonstrate how the empty carrier kinetics can influence cotransport function, we used the eight-state model to simulate the observed behavior for the G134C mutant. Minor changes to the model parameters would also allow prediction of the M533C behavior. The starting point for our simulations was based on the estimates of the apparent valency and rate constants for G134C + MTS in ND0 (Table I) of the main detectable presteady-state relaxation. In the model, these rates correspond to the empty carrier transition rates at $V = 0$ (k_{18}^0 and k_{81}^0). Other rate constants were chosen to give the observed steady-state activation behavior in terms of the apparent affinity for P_i (~0.05 mM) and for Na^+ (~40–50 mM) and the chord slope of the steady-state P_i activation I–V data in the range −100 to 0 mV. We assumed that all transitions were operating under nonrapid equilibrium conditions and only the empty carrier (1–8) and first Na^+ binding (1–2) transitions were voltage dependent and each could be described by one kinetic step (and assuming sharp energy barriers) (e.g., Parent et al., 1992, Loo et al., 2002).

As illustrated in Fig. 7 B, we could simulate the effect of MTS on the main presteady-state relaxations for G134C, observed in ND0 and ND100, by changing only the rate constants of the empty carrier transition at $V = 0$. The rate constants for G134C − MTS differed slightly from those in Table I, which most likely reflects uncertainties in the exponential fitting due to noise or artifacts at extreme test potentials and the simplification of the empty carrier kinetics to a single transition. The simulated data show that for a ±120-mV voltage step from −60 mV, there is less charge movement in the hyperpolarizing direction in the G134C − MTS condition compared with the depolarizing step, whereas the charge movement becomes more symmetrically distributed in the G134C + MTS condition (Fig. 4 C). The simulations also predict that in ND100, a fast component is introduced by the Na^+ binding/debinding transition (1–2) that is most easily seen for the −MTS simulation. As indicated by the vertical bars superimposed on the traces of Fig. 7 B, the time window used for the presteady-state analysis in this study precluded characterization of this component from the experimental data. Quantification of fast relaxing components ($\tau \sim$ 1–2 ms) using the two-electrode voltage clamp is also dependent on the speed and homogeneity of the oocyte membrane voltage control, as well as the recording signal-to-noise ratio and expression level. The simulated presteady-state relaxations were quantitated in terms of the time constant of the main relaxation (τ_{ON}) (Fig. 7 C) and the charge moved by voltage steps (Q_{ON}) (Fig. 7 D). The τ_{ON}–V data reflect the same behavior observed for G134C (Fig. 5 A), whereby a hyperpolarizing shift in the maximum occurs for the +MTS case. The simulated Q_{ON}–V data also recapitulate the behavior of the measured data (Fig. 6 A), whereby for G134C − MTS, the charge movement saturates in the hyperpolarizing direction and there is only a marginal increase in charge movement due to the presence of 100 mM Na^+.

The simulated steady-state I–V data for I_{P_i} (Fig. 7 E), assuming 1 mM P_i and 100 mM Na^+, indicated that changes to k_{18}^0 and k_{81}^0 could account for an altered voltage dependency of I_{P_i} for G134C − MTS (or M533C + MTS), but not the reduced maximum turnover rate (Fig. 1 E). We took account of this in our model by reducing the fully loaded carrier transition k_{45}. To simulate the behavior of M533C + MTS, k_{45} would have to be further reduced to account for smaller steady-state activity (Fig. 1 E). Lastly, we determined the voltage dependency of the apparent substrate affinities (K_m^{Pi} and K_m^{Na}) (Fig. 7 F) by simulating steady-state I–V data with the same substrate concentrations used experimentally and fitting the simulated data with a Michaelis-Menten function (Eq. 1) for the $K_m^{P_i}$ determination and the modified Hill equation (Eq. 2) for the K_m^{Na} determination. From the fit to the Na^+ activation data, the Hill coefficient for the −MTS case

increased from 2.0 (−100 mV) to 2.5 (0 mV), and for the +MTS case, it increased from 2.1 (−100 mV) to 2.4 (0 mV). As shown in Fig. 7 F, both $K_m^{P_i}$ and K_m^{Na} decreased with hyperpolarization; however, for $K_m^{P_i,i}$ for the +MTS case, it was approximately twofold larger at all potentials. Interestingly, we also observed a similar trend in the estimates of $K_m^{P_i}$ and K_m^{Na} reported by the fitting algorithm, which, despite the uncertainties in the estimates of these parameters from the experimental data, confirms the robustness of the model to describe the transport activity.

Overall, the simulations suggest that the empty carrier rates (k_{18} and k_{81}) are crucial determinants of the NaPi-IIa kinetics. At any *V*, they define the probability of occupying a given state, in particular, the occupancy of state 2, which precedes P_i binding and subsequent cotransport. Fig. 8 shows the voltage dependency of occupancies of the predominantly occupied states for three superfusion conditions: ND0, ND100, and ND100 + 1 mM P_i. In ND0, the simulation predicts that for G134C − MTS (or M533C + MTS), the empty carrier remains mostly in state 1 for hyperpolarizing potentials. This would correspond to an outward-facing conformation of the protein. For G134C + MTS (or M533C − MTS), the empty carrier is distributed between states 1 and 8 and this distribution is shifted to predominantly state 1 only for extreme hyperpolarizing potentials. In ND100 for the −MTS condition, the probability of occupying state 8 is low, and the carrier occupancy moves from state 1 to state 2 as the probability of Na^+ binding increases with hyperpolarization. The charge movement contributed by the empty carrier would be small for hyperpolarizing steps for this condition, with the rapid Na^+ binding transition (1–2) contributing most of the charge movement. In contrast, for the +MTS condition, the transporter must first leave state 8 (inward facing, empty carrier) to reach state 2 via the intermediate state 1. Compared with the −MTS condition, we would expect this to involve a much larger structural reorientation for a given change in *V* and concomitant charge movement for hyperpolarizing steps. Finally, in the presence of saturating P_i, the main states occupied are 4 (fully loaded carrier, outward facing) and 8 (empty carrier, inward facing). The voltage dependency of the state 4 occupancy now reflects the steady-state *I–V* data for each condition; for −MTS, state 4 is preferred at hyperpolarizing potentials, whereas for +MTS, the transporter is distributed between states 4 and 8 depending on *V*. The voltage-dependent shift in the occupancies of states 4 and 8 for +MTS is also reflected in the stronger voltage dependency of $K_m^{P_i}$ for this condition (Fig. 7 F). A qualitatively similar trend is also predicted for K_m^{Na}; however, this parameter is also a strong function of the final Na^+ binding transition that is assumed to involve a

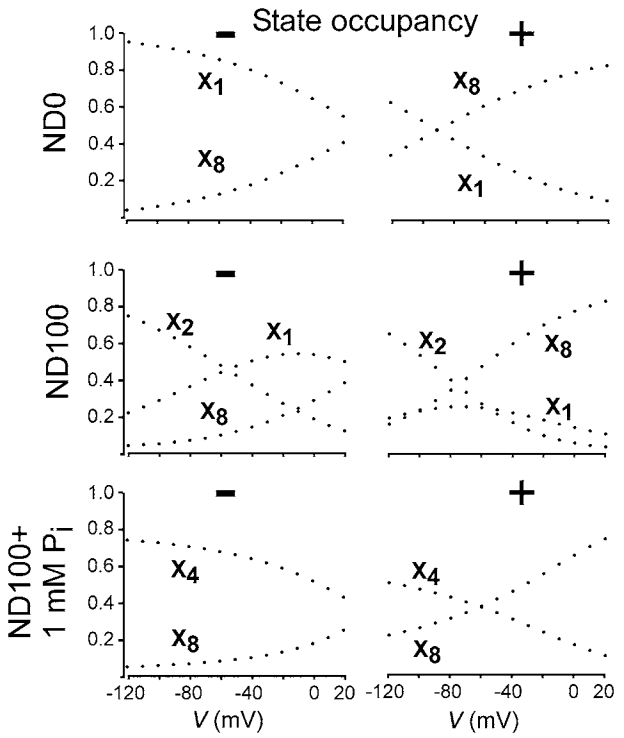

FIGURE 8. Simulations of occupancy of states 1, 2, 4, and 8 of the model scheme depicted in Fig. 7 A, as a function of membrane potential in zero external Na^+ (ND0), 100 mM external Na^+ (ND100), and 100 mM external Na^+ with 1 mM P_i (ND100 + 1 mM P_i), before (−) and after (+) modification of Cys-134.

highly cooperative binding of two Na^+ ions (Forster et al., 1998, 2000).

The behavior of WT NaPi-IIa corresponds closely to that of G134C + MTS (or M533C − MTS) in which the preferred orientation of the empty carrier in the absence of external Na^+ and $V = 0$ is inward facing and this can be altered by membrane hyperpolarization to the outward-facing conformation. A similar situation has been described by Loo et al. (2002) for the sodium glucose cotransporter SGLT-1, whereby the empty carrier is predicted to undergo a voltage-dependent reorientation from inward to outward conformation for hyperpolarizing *V*. This behavior suggests a common voltage-dependent mechanism for these Na^+-coupled cotransport systems. Moreover, it is consistent with alternating access schemes for membrane transport proteins in which large conformational changes occur to the empty carrier that would alternately offer accessibility of the substrate binding sites to the cytosol or external medium (Loo et al., 1998, 2002). For NaPi-IIa, the state occupancy is also a strong function of external protons (Forster et al., 2000); the action of which on the empty carrier kinetics can be emulated by the molecular manipulations performed at sites Gly-134 and Met-533. The altered preferred orientation of the carrier for G134C − MTS and M533C + MTS can also ex-

plain their increased sensitivity of cotransport activity to external protons, as this would presumably increase proton accessibility to the Na^+ binding sites.

Structure–Function Implications

In summary, the effect of introducing a Cys at Gly-134 or MTS modification of Cys-533 is to stabilize the empty carrier conformation so that it is increasingly likely to occupy the outward-facing conformation for $V < 0$. Thus, we have been able to alter the preferred orientation of the empty carrier through cys substitution or cys modification or both, depending on the linker region. The proposed interactions of the modified sites with the voltage-dependent parts of NaPi-IIa reveal a novel structure–function relationship; functionally, they result in modified steady-state cotransport kinetics that correlate with changes to the presteady-state kinetics. When incorporated into an alternating access model for NaPi-IIa, the altered rate constants of the presteady-state charge movements indicate that these interactions induce major voltage-dependent reorientations of the protein structure.

In the absence of 3-D structural data for NaPi-IIa, we can only speculate how the Cys engineering at sites 134 and 533 could lead to the functional behavior documented in this study. Based on previous cys mutagenesis studies (Lambert et al., 2001, Kohler et al., 2002a,b), we have proposed that sites in ECL-3 and ICL-1 contribute to a cotransport pathway through NaPi-IIa, possibly by forming two reentrant loops in a common hydrophilic vestibule. This is also consistent with NaPi-IIa being a functional monomer (Kohler et al., 2000) and the requirement that the COOH-terminal and NH_2-terminal halves of the protein together form a functional transporter (Ehnes et al., 2002). These halves are most likely stabilized by two disulfide bridges (Kohler et al., 2003), which thereby place constraints on the spatial relationship of the predicted transmembrane domains. Major conformational changes are assumed to occur during the transport cycle according to the alternating access model, as proposed for the recently crystallized GlpT and LacY transporters (Abramson et al., 2003; Huang et al., 2003). For NaPi-IIa, we speculate that these involve movement of TMD-2/TMD-3 associated with ICL-1 in the NH_2-terminal half and TMD-5/TMD-6 associated with ECL-3 in the COOH-terminal half. Gly-134 would confer the necessary flexibility to ECL-1 for TMD-2 to adopt inward and outward-facing conformations according to the alternating access scheme, depending on the membrane potential. Cys substitution at 134 might constrain these movements and stabilize the outward-facing conformation, as predicted from the simulations. This preferred orientation would also hinder the substrate translocation transition in agreement with the slower rate for partial reaction 4–5 (Fig. 7 A). Addition of a bulky MTS reagent to this Cys would destabilize the protein to restore a WT-like inward-facing conformation. In the COOH-terminal half of the protein, the Met-533-Cys substitution is well tolerated, but when Cys-533 is modified, the additional bulk of the MTS reagent could now sterically hinder movements of TMD-6, for example, so that the protein adopts an outward-facing conformation similar to that induced by Cys-134.

We thank Dr. Don Loo (University of California at Los Angeles, Los Angeles, CA) for valuable discussions on the interpretation of the voltage dependency mechanism and Dr. Leila Virkki (University of Zurich) for helpful comments on the manuscript.

This work was supported by grants to H. Murer from the Swiss National Science Foundation (31-46523), the Hartmann Müller-Stiftung (Zurich), the Olga Mayenfisch-Stiftung (Zurich), and the Union Bank of Switzerland (Zurich) (Bu 704/7-1).

Lawrence G. Palmer served as editor.

Submitted: 12 March 2004
Accepted: 14 September 2004

REFERENCES

Abramson, J., I. Smirnova, V. Kasho, G. Verner, H.R. Kaback, and S. Iwata. 2003. Structure and mechanism of the lactose permease of *Escherichia coli*. *Science*. 301:610–615.

Ehnes, C., I.C. Forster, K. Kohler, J. Biber, and H. Murer. 2002. Functional studies on a split type II Na/P(i)-cotransporter. *J. Membr. Biol.* 188:227–236.

Ehnes, C., I.C. Forster, K. Kohler, A. Bacconi, G. Stange, J. Biber, and H. Murer. 2004. Structure–function relations of the first and fourth predicted extracellular linkers of the type IIa Na^+/Pi cotransporter. I. cysteine scanning mutagenesis. *J. Gen. Physiol.* 124:475–488.

Forster, I., J. Biber, and H. Murer. 2000. Proton-sensitive transitions of renal rat type II Na^+-coupled phosphate cotransporter kinetics. *Biophys. J.* 79:215–230.

Forster, I., N. Hernando, J. Biber, and H. Murer. 1998. The voltage dependence of a cloned mammalian renal type II Na^+/P_i cotransporter (NaPi-2). *J. Gen. Physiol.* 112:1–18.

Forster, I.C., C.A. Wagner, A.E. Busch, F. Lang, J. Biber, N. Hernando, H. Murer, and A. Werner. 1997. Electrophysiological characterization of the flounder type II Na^+/Pi cotransporter (NaPi-5) expressed in *Xenopus laevis* oocytes. *J. Membr. Biol.* 160:9–25.

Hartmann, C.M., C.A. Wagner, A.E. Busch, D. Markovich, J. Biber, F. Lang, and H. Murer. 1995. Transport characteristics of a murine renal Na/Pi-cotransporter. *Pflugers Arch.* 430:830–836.

Hazama, A., D.D. Loo, and E.M. Wright. 1997. Presteady-state currents of the rabbit Na^+/glucose cotransporter (SGLT1). *J. Membr. Biol.* 155:175–186.

Huang, Y., M.J. Lemieux, J. Song, M. Auer, and D.N. Wang. 2003. Structure and mechanism of the glycerol-3-phosphate transporter from *Escherichia coli*. *Science*. 301:616–620.

Kohler, K., I.C. Forster, G. Lambert, J. Biber, and H. Murer. 2000. The functional unit of the renal type IIa Na^+/P_i cotransporter is a monomer. *J. Biol. Chem.* 275:26113–26120.

Kohler, K., I.C. Forster, G. Stange, J. Biber, and H. Murer. 2002a. Identification of functionally important sites in the first intracellular loop of the NaPi-IIa cotransporter. *Am. J. Physiol. Renal Physiol.* 282:F687–F696.

Kohler, K., I.C. Forster, G. Stange, J. Biber, and H. Murer. 2002b.

Transport function of the renal type IIa Na^+/P_i cotransporter is codetermined by residues in two opposing linker regions. *J. Gen. Physiol.* 120:693–705.

Kohler, K., I.C. Forster, G. Stange, J. Biber, and H. Murer. 2003. Essential cysteine residues of the type IIa Na^+/Pi cotransporter. *Pflugers Arch.* 446:203–210.

Lambert, G., I.C. Forster, G. Stange, J. Biber, and H. Murer. 1999. Properties of the mutant Ser-460-Cys implicate this site in a functionally important region of the type IIa Na^+/P_i cotransporter protein. *J. Gen. Physiol.* 114:637–652.

Lambert, G., I.C. Forster, G. Stange, K. Kohler, J. Biber, and H. Murer. 2001. Cysteine mutagenesis reveals novel structure–function features within the predicted third extracellular loop of the type IIa Na^+/P_i cotransporter. *J. Gen. Physiol.* 117:533–546.

Loo, D.D., B.A. Hirayama, E.M. Gallardo, J.T. Lam, E. Turk, and E.M. Wright. 1998. Conformational changes couple Na^+ and glucose transport. *Proc. Natl. Acad. Sci. USA.* 95:7789–7794.

Loo, D.D.F., S. Eskandari, B.A. Hirayama, and E.M. Wright. 2002. A kinetic model for secondary active transport. *In* IMA Volumes in Mathematics and Its Applications. Volume 129: Membrane Transport and Renal Physiology. H.E. Layton and A.M. Weinstein, editors. Springer Verlag, New York. 1–19.

Parent, L., S. Supplisson, D.D. Loo, and E.M. Wright. 1992. Electrogenic properties of the cloned Na^+/glucose cotransporter. II. A transport model under nonrapid equilibrium conditions. *J. Membr. Biol.* 125:63–79.

Rakowski, R.F. 1993. Charge movement by the Na/K pump in *Xenopus* oocytes. *J. Gen. Physiol.* 101:117–144.